Triarylporphyrin *meso*-Oxy Radicals: Remarkable Chemical Stabilities and Oxidation to Oxophlorin π-Cations

Daiki Shimizu,[†] Juwon Oh,[‡] Ko Furukawa,*,[§] Dongho Kim,*,[‡] and Atsuhiro Osuka*,[†]

[†]Department of Chemistry, Graduate School of Science, Kyoto University, Sakyo-ku, Kyoto 606-8502, Japan
[‡]Spectroscopy Laboratory for Functional π-Electronic Systems and Department of Chemistry, Yonsei University, Seoul 120-749, South Korea
[§]Center for Instrumental Analysis, Niigata University, Nishi-ku, Niigata 950-2181, Japan

Ⓢ *Supporting Information*

ABSTRACT: 5-Hydroxy-10,15,20-triarylporphyrin (oxophlorin) and its Ni(II) and Zn(II) complexes were oxidized with PbO_2 to give the corresponding porphyrin *meso*-oxy radicals as remarkably stable species. These radicals were fully characterized with X-ray diffraction analysis, UV/vis/NIR absorption and ESR spectroscopies, magnetic susceptibility measurement, electrochemical studies, and theoretical calculations. Free-base radical and its Ni(II) complex have been shown to exist as a monoradical in solution, while the Zn(II) complex exists in an equilibrium between monomer (doublet monoradical) and dimer (a non-Kekulé singlet biradicaloid) with a dimerization constant of $K_D = 3.0 \times 10^5$ M^{-1} in noncoordinating CH_2Cl_2 but becomes a pyridine-coordinated monoradical upon addition of pyridine. Variable temperature magnetic susceptibility measurements of these radicals revealed different magnetic interactions in the solid-states, which has been interpreted in terms of their different packing structures in a microscopic sense. These radicals undergo one-electron oxidation and reduction in a reversible manner within narrow potential windows of 0.57−0.82 V. Finally, one-electron oxidation of Ni(II) and Zn(II) porphyrin *meso*-oxy radicals with tris(4-bromophenyl)aminium hexachloroantimonate furnished oxophlorin π-cations, which displayed nonaromatic closed-shell character, NIR absorption, and significant double bond character of the C−O bond.
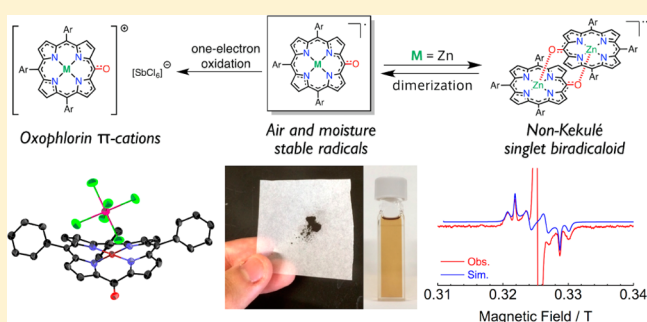
■ INTRODUCTION

Over the last decade or so, organic stable radicals have increasingly grown as a new class of functional molecules because of their intriguing properties originating from open-shell electronic systems.[1] The electronic, optical, and magnetic properties of open-shell molecules are quite different from those of closed-shell molecules, encouraging their potential uses in various fields, such as organic synthesis,[2a] polymer chemistry,[2b] magnetic materials,[2c] organic batteries,[2d] quantum information science,[2e] and bioimaging.[2f] However, open-shell electronic structures usually lead to high reactivities and instabilities, making their manipulations very difficult. Therefore, exploration of novel stable organic radicals has still remained a big challenge in current organic chemistry. It is desirable that such stable organic radicals are easily synthesized from simple precursors in large scale and amenable to versatile fabrications to meet required functions.

Oxophlorin **1a**,[3] a tautomeric pair of *meso*-hydroxyporphyrin **1b**, was investigated in light of its important roles in heme catabolism. It has been widely accepted that the heme catabolism sequence starts with *meso*-hydroxylation of heme by heme oxygenase.[4] To obtain detailed insights on the biological mechanism, octaethylporphyrin (OEP) derivatives have been employed as a synthetic model of hemes.[5] It was

already reported in 1970 that OEP-type oxophlorin contains ca. 1% of paramagnetic species,[6] but it had taken a long time until the first structural characterization of the paramagnetic species, oxophlorin radical, was reported.[7a] As a remarkable breakthrough of these studies, Balch et al. isolated OEP-type oxophlorin radicals **2M-py** by aerobic oxidation of oxophlorin in the presence of pyridine and succeeded in X-ray crystal structural determination (Chart 1).[7,8] It was also reported by Fuhrhop and Besecke that coordination of pyridine to the metal center was mandatory to suppress the formation of a C(15)−C(15′) linked oxophlorin dimer.[9] Later, Smith et al. improved the chemical stability of the radical by introducing a *tert*-butyl group at the 15-position, where the highest spin density was expected. Compound **3** was certainly stable without coordination of a base, but underwent 30% degradation after storage for 2 weeks in solution.[10] They further used this synthetic strategy to construct shape-persistent *meso*−*meso* linked oxophlorin oligomers in an elegant manner.[11] The electronic structures of oxophlorin radicals and their metal complexes were examined by theoretical calculations.[12]
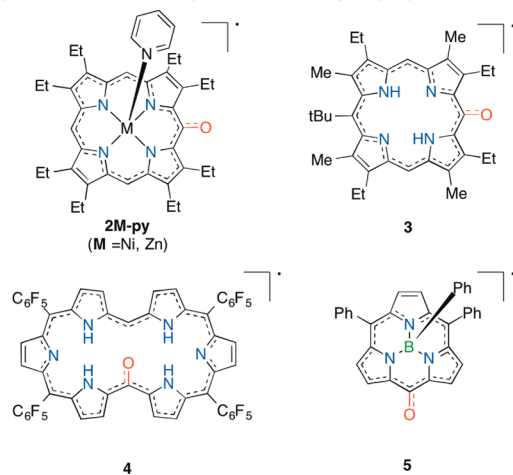
Chart 1. Oxophlorin and Isolated Radical Species Based on Oxophlorin Derivatives

Oxophlorin and its radical species
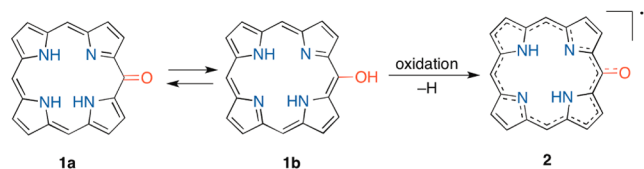
Reported meso-oxy radicals of porphyrinoids


Besides these studies, *meso*-aryl substituted porphyrinoids have emerged as a new platform to effectively stabilize radicals either as π-radicals or *meso*-oxy radicals. Hexaphyrin *meso*-oxy radical **4** (Chart 1) was reported to be very stable, and it was handled under ambient conditions and purified over a usual silica gel column.[13] The observed particular stability of **4** has been explained in terms of the full delocalization of a spin over the whole hexaphyrin electronic network and the steric protection of the radical center that is well embedded in the hexaphyrin interior. Quite recently, we found that subporphyrin *meso*-oxy radical **5** (Chart 1) was also an extremely stable radical, in which a spin is nicely delocalized over the whole molecule, including the *meso*-aryl groups.[14] In addition, the *meso*-aryl groups in **5** are considered to sterically protect the *meso*-positions, where the spin densities are relatively high. With this background, it occurred to us that 10,15,20-triaryl-substituted porphyrin *meso*-oxy radicals might also be stable. While these radical species have simple structures and are easy to synthesize, there has been no study on these molecules to date. Here, we report that 10,15,20-triaryl porphyrin *meso*-oxy radicals are extremely stable and can be manipulated like usual closed-shell organic molecules. Porphyrins are characterized by intense absorption and emission in the ultraviolet, visible, and near-infrared spectral regions. The ability of porphyrins to coordinate metal cations allows for versatile tuning of their properties. The planar and rigid structures of porphyrins make them attractive building blocks for the construction of self-assembled structures. Considering these favorable attributes of porphyrins, 10,15,20-triaryl porphyrin *meso*-oxy radicals are promising synthetic building blocks of new functional systems.

■ RESULTS AND DISCUSSION

Synthesis. *meso*-Hydroxy-substituted Ni(II) porphyrin **7Ni** was synthesized in 82% yield by Pd-catalyzed hydroxylation of

meso-bromoporphyrin **6Ni** by modifying the previous methods reported by Senge and Arnold.[15] They suggested the generation of a trace amount of radical species via aerobic oxidation of **7Ni** on the basis of broadening of its ^{1}H NMR spectrum,[15] but the isolation and characterization of radical species were not attempted. We thus reexamined the isolation of TPP-type porphyrin *meso*-oxy radicals. Demetalation of **7Ni** to its free-base porphyrin **7H$_2$** was achieved in 97% yield upon treatment with H$_2$SO$_4$/CF$_3$CO$_2$H. Zn(II) complex **7Zn** was prepared by treating **7H$_2$** with Zn(OAc)$_2$ in 83% yield (Scheme 1, top). We confirmed that the ^{1}H NMR spectra of these *meso*-

Scheme 1. Synthesis of *meso*-Oxy Porphyrin Radicals^a
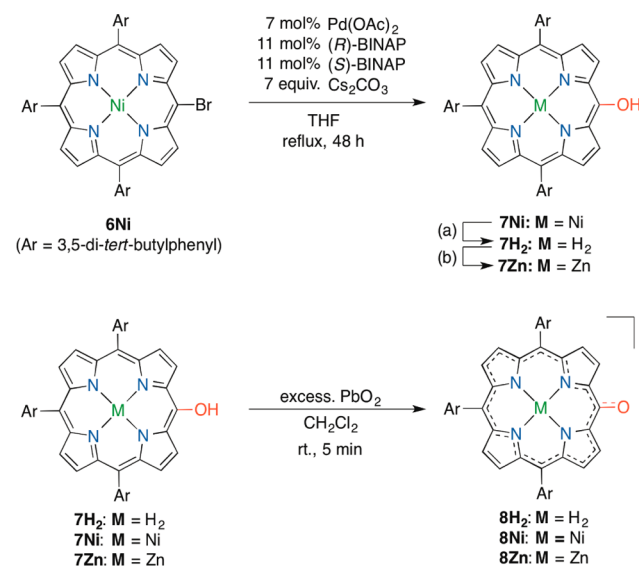
^{a}Reagents and conditions: (a) H$_2$SO$_4$/CF$_3$CO$_2$H, 0 °C, 30 min, 97%; (b) Zn(OAc)$_2$, CH$_2$Cl$_2$/MeOH, rt., 2 h, 83%.

hydroxyporphyrins were broadened and poorly resolved except for two singlets due to the *tert*-butyl groups, most probably owing to the presence of a small amount of radial species in solution. In line with this conjecture, the ^{1}H NMR spectrum became sharpened upon addition of an excess amount of hydrazine monohydrate. These experiments indicated that *meso*-hydroxyporphyrins were relatively easily oxidized under air to give porphyrin *meso*-oxy radicals, which were cleanly reduced to give *meso*-oxy anions upon treatment with hydrazine. Clearer ^{1}H NMR spectra of *meso*-hydroxyporphyrins with hydrazine monohydrate were taken in DMSO, which prevented intermolecular hydrogen bonding (e.g., Figure S1-2 in the Supporting Information, SI).[16] High-resolution atmospheric-pressure-chemical-ionization time-of-flight mass spectrometry (HR-APCI-TOF-MS) exhibited precursor cation peaks of **7H$_2$** at m/z = 891.5913 (calcd. 891.5935 for [**7H$_2$**+H]$^+$; [C$_{62}$H$_{75}$N$_4$O]$^+$), **7Ni** at m/z = 947.5085 (calcd. 947.5132 for [**7Ni**+H]$^+$; [C$_{62}$H$_{73}$N$_4$O^{58}Ni]$^+$), and **7Zn** at m/z = 952.4956 (calcd. 952.4992 for [**7Zn**]$^+$; [C$_{62}$H$_{72}$N$_4$O^{64}Zn]$^+$).

Oxidations of these *meso*-hydroxyporphyrins to the corresponding *meso*-oxy radials were quantitatively accomplished upon treatment with PbO$_2$ in CH$_2$Cl$_2$ at room temperature. The colors of *meso*-hydroxyporphyrins changed immediately upon treatment with PbO$_2$. Simple filtration followed by recrystallization gave the corresponding *meso*-oxy radicals **8H$_2$**, **8Ni**, and **8Zn** in 86, 91, and 89% yields, respectively (Scheme 1, bottom). These radicals have been structurally well charac-

terized by X-ray single crystal diffraction analyses, which have revealed that **8H$_2$** and **8Ni** are monomeric radicals but Zn(II) porphyrin *meso*-oxy radical **8Zn** forms a face-to-face dimer, **9Zn** (Scheme 2).[17] It is important to note that **9Zn** is not a closed-

Scheme 2. Formation of a Face-to-Face Dimer 9Zn
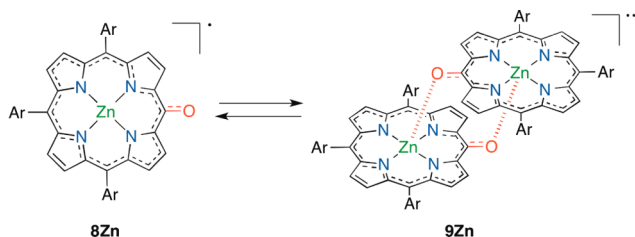
shell spin-recombined dimer but a coordination dimer having two radical centers. The structural details will be discussed later. Alternatively, recrystallization of **9Zn** in the presence of pyridine gave pyridine-coordinated monomer **8Zn-py** quantitatively as a brown solid. HR-APCI-TOF-MS exhibited the respective monomeric porphyrin cation peaks of **8H$_2$** at m/z = 890.5825 (calcd. 890.5857 for [**8H$_2$** + H]$^+$; [C$_{62}$H$_{74}$N$_4$O]$^+$),

8Ni at m/z = 946.5074 (calcd. 946.5054 for [**8Ni** + H]$^+$; [C$_{62}$H$_{72}$N$_4$O^{58}Ni]$^+$), and **8Zn** at m/z = 951.4900 (calcd. 951.4914 for [**8Zn**]$^+$; [C$_{62}$H$_{71}$N$_4$O^{64}Zn]$^+$). High-resolution electrospray-ionization time-of-flight mass spectrometry (HR-ESI-TOF-MS) as a milder ionization method than APCI revealed the parent anion peak of **9Zn** at m/z = 1902.9781 (calcd. 1902.9844 for [**9Zn**]$^-$; [C$_{124}$H$_{142}$N$_8$O$_2$^{64}Zn$_2$]$^-$), confirming the formation of **9Zn**. The ^{1}H NMR spectra of these radical species gave no signals except for two singlets due to the *tert*-butyl groups, and active signals were observed by ESR spectroscopy (*vide infra*). Importantly, these radicals are fairly stable under ambient conditions both in the solid states and in solutions. These radicals can be purified by silica gel column chromatography, and can be stored for months without deterioration in the solid states, and they survive for several weeks in C$_6$D$_6$ solutions.

X-ray Crystallographic Analysis. Single crystal X-ray diffraction analysis on **7Ni** revealed its planar structure, as indicated by a small mean plane deviation (MPD) value (0.096 Å), defined by 24 atoms and a C—O bond length of 1.349(8) Å, both of which are similar to those of previously reported *meso*-hydroxy Ni(II) porphyrins.[15] The structure of **8H$_2$** shows a
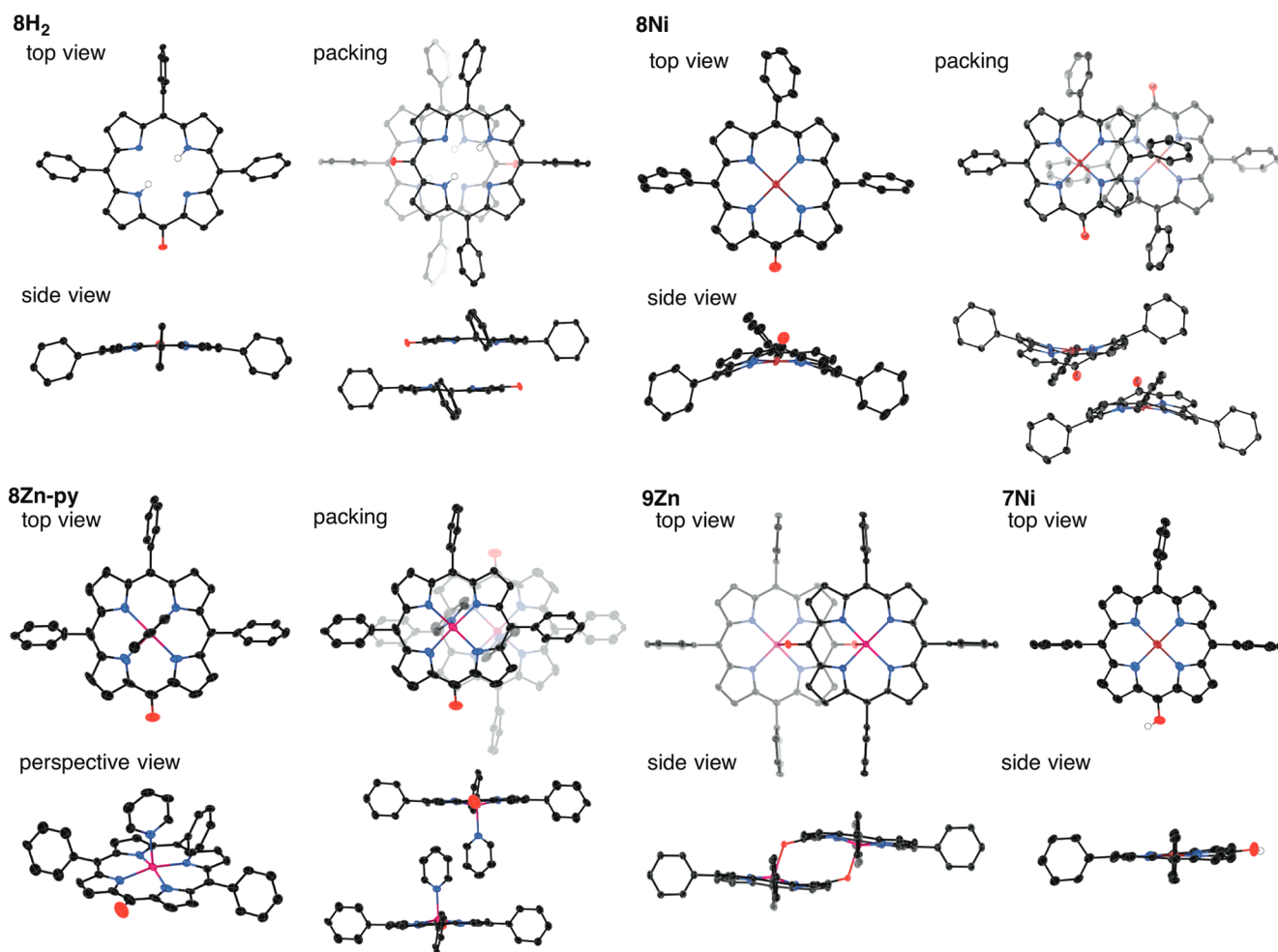

Figure 1. X-ray crystal structures of **8H$_2$**, **8Ni**, **8Zn-py**, and **9Zn**, and **7Ni**. Thermal ellipsoids are scaled to the 50% probability level. Solvent molecules; hydrogen atoms, except for the inner NHs of **8H$_2$** and the *meso*-OH of **7Ni**; and *tert*-butyl groups are omitted for clarity. Selected bond lengths: C5—O: 1.349(8) Å for **7Ni**, 1.223(4) Å for **8H$_2$**, 1.238(3) Å for **8Ni**, 1.289(7) Å for **8Zn-py**, 1.267(2) Å for **9Zn**; Zn—N(5): 2.130(4) Å for **8Zn-py**; Zn—O: 2.1478(14) Å for **9Zn**. Mean plane deviations are 0.096 Å for **7Ni**, 0.075 Å for **8H$_2$**, 0.358 Å for **8Ni**, 0.041 Å for **8Zn-py**, and 0.087 Å for **9Zn**.

small MPD value of 0.075 Å. Characteristically, the C−O bond length in **8H₂** is 1.233(4) Å, which is distinctly shorter as compared with the typical C−O single bond lengths (1.3−1.4 Å). This strongly suggests a significant double bond character for the C−O bond of **8H₂** and, hence, effective spin delocalization over the porphyrin ring. In the crystal, two molecules of **8H₂** form an antiparallel offset face-to-face dimer with an interporphyrin separation of 3.354 Å.[18] Ni(II) porphyrin *meso*-oxy radical **8Ni** shows a more bent saddle-like conformation with a MPD value of 0.358 Å and a short C−O bond length of 1.238(3) Å. The radical **8Ni** also forms an offset face-to-face dimer at the convex face. In **8Ni**, the C−O bonds are directed perpendicular to the long molecular axis. The closest interporphyrin separation is short, being only 3.190 Å between C(4) and C(13)′ atoms. Pyridine-coordinated Zn(II) porphyrin *meso*-oxy radical **8Zn-py** displays a more planar structure of a small MPD value of 0.041 Å and a short C−O bond length of 1.289(7) Å. This radical also forms a dimer in the crystal, but the coordinated pyridines are positioned between the two porphyrins, separating Zn(II) porphyrins apart by 8.563 Å. The structure of dimeric Zn(II) porphyrin *meso*-oxy radical **9Zn** is constructed from complementary coordination of the oxygen atom to the Zn atom in the porphyrin pocket. The C−O bond length is 1.267(2) Å, and the Zn−O length of **9Zn** is 2.148(1) Å, which is significantly shorter than the sum of van der Waals radii (2.91 Å). An averaged interporphyrin distance is relatively short, being 3.112 Å, which is caused by bonding interaction between the Zn and O atoms.

Optical Properties. The UV/vis absorption spectra of **7H₂**, **7Ni**, and **7Zn** in THF show intense Soret bands around 420 nm and weak Q-bands around 550 nm with some vibronic structures, as seen for typical porphyrins (Figure 2a). The absorption spectrum of **7H₂** is highly dependent upon the solvents, probably reflecting the relative contribution of *meso*-hydroxyporphyrin and oxophlorin. The *meso*-hydroxyporphyrin form is predominant in THF, acetone, and hexane, while the oxophlorin form is more important in CH₂Cl₂ and methanol (Figure S4-2). Porphyrins **7H₂** and **7Zn** in THF emit fluorescence with maxima at 663 and 610 nm as mirror images of their Q-bands with fluorescence quantum yields of 0.064 and 0.081, respectively.

The UV/vis/NIR absorption spectrum of monoradical **8H₂** in CH₂Cl₂ shows a Soret-like band at 420 nm and Q-like bands at 480, 535, 576, and 815 nm, along with weak and broad bands with peaks at 1123 and 1312 nm that are characteristic of porphyrinoid radicals (Figure 2b). The absorption spectrum of **8Ni** in CH₂Cl₂ is similar to that of **8H₂**, featuring a Soret-like band at 437 nm and Q-like bands at 497, 582, 807, and 1134 nm, along with weak and broad bands with peaks at 1332 and 1621 nm. Similar to the absorption spectra of **8H₂** and **8Ni**, monomeric Zn(II) porphyrin *meso*-oxy radical **8Zn-py** shows the absorption spectrum that contains a Soret-like band at 438 nm, Q-like bands at 492, 598, and 860 nm, together with broad and red-shifted bands at 1149 and 1367 nm. As will be discussed later, TD-DFT calculations predicted that the low energy absorption bands observed for **8H₂**, **8Ni**, and **8Zn-py** correspond to HOMO−SOMO and SOMO−LUMO transitions.

Different from the absorption spectra of **8H₂**, **8Ni**, and **8Zn-py**, the absorption spectrum of pyridine-free Zn(II) porphyrin *meso*-oxy radical **8Zn** in CH₂Cl₂ shows concentration dependent spectral changes, as shown in Figure 2c. The absorption
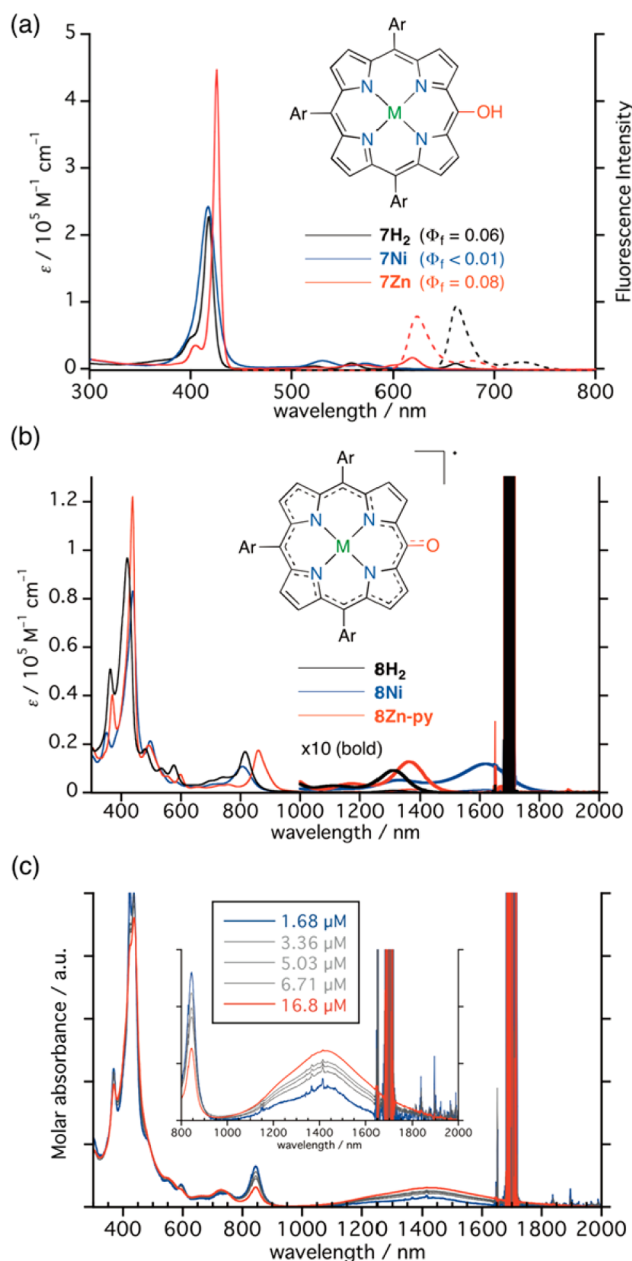

Figure 2. (a) UV/vis absorption (solid) and emission (dashed) spectra of **7H₂**, **7Ni**, and **7Zn** in THF. (b) Absorption spectra of **8H₂**, **8Ni**, and **8Zn-py** in CH₂Cl₂. (c) Concentration dependent absorption spectra of **9Zn** in CH₂Cl₂.

spectrum of **8Zn** at a low concentration (1.68 μM) shows a spectral pattern that is similar to those of the monomeric **8H₂**, **8Ni**, and **8Zn-py** species, but that at a high concentration (16.8 μM) exhibits a drastically different spectral pattern with a broad and strong band at 1450 nm, which has been assigned to dimeric **9Zn**. The concentration-variable absorption spectra of **8Zn** display systematic changes with an isosbestic point around 900 nm, indicating an equilibrium between **8Zn** and **9Zn** with an association constant of 3.0×10^5 M^{-1} in CH₂Cl₂ at 298 K, and the molar absorption coefficient of 7.0×10^3 M^{-1} cm^{-1} at 1450 nm for **9Zn** (see Figure S4-5 in the SI for the detailed calculation). From the association constant, the binding energy between two chromophores in **9Zn** is determined to be 31.2 kJ mol^{-1} at 298 K. The characteristic absorption band around 1450 nm is considered to be the intramolecular charge transfer
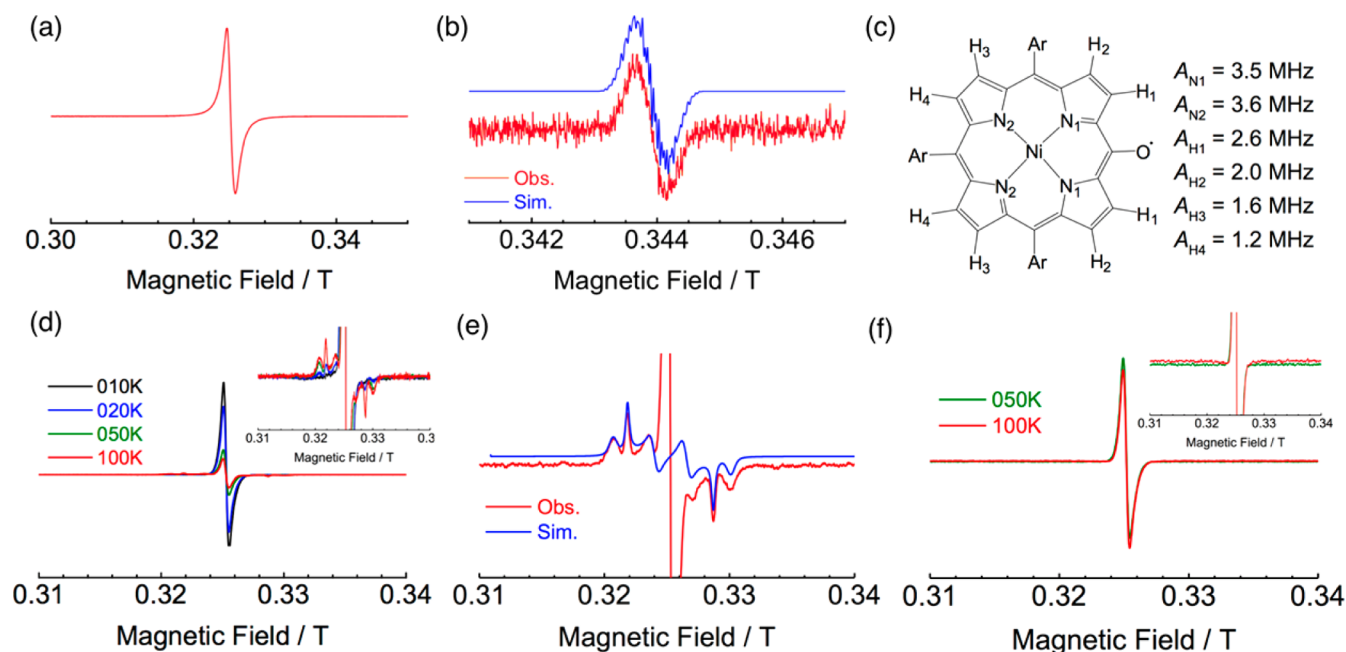
Figure 3. (a) ESR spectrum of **8H$_2$** (in toluene, 1.0 mM at room temperature). (b) Observed and simulated ESR spectra of **8Ni** (in toluene, 0.1 mM at room temperature). (c) Simulated hyperfine coupling constants for **8Ni**. (d) VT-ESR spectra of an equilibrium solution between **8Zn** and **9Zn** in toluene at 1.15 mM. (e) Comparison of the observed ESR spectrum of **8Zn** and **9Zn** at 100 K with the simulated ESR spectrum of **9Zn**. (f) VT-ESR spectra of **8Zn-py** in a toluene/pyridine solution.

(CT) band. The excitation energy was estimated to be 0.62 eV on the basis of the absorption terminal ca. 2000 nm, which is consistent with the observed electrochemical oxidation−reduction gap (0.57 eV, see below). Addition of pyridine completely dissociated **9Zn** to pyridine coordinating complex **8Zn-py**, which gave a similar spectrum to those of **8H$_2$** and **8Ni**.

Magnetic Properties. The magnetic properties of the radicals were evaluated with electron spin resonance (ESR) spectroscopy in degassed toluene solutions. The ESR spectrum of **8H$_2$** and **8Ni** showed signals at g = 2.0028 and 2.0035, respectively (Figure 3a,b). The hyperfine coupling constants were determined for **8Ni** at room temperature. The obtained hyperfine coupling constants from spectral simulation (Figure 3c) revealed effective spin delocalization over the macrocycle along with almost no delocalization over the *meso*-substituents and the Ni center. It is worth noting that hyperfine splitting of these ESR spectra of porphyrin *meso*-oxy radicals was significantly smaller than that of subporphyrin *meso*-oxy radical **5**, indicating that spin delocalization of *meso*-oxy radical is more effective in subporphyrin than in porphyrin. The ESR spectrum of the zinc complex in a 1.15 mM toluene solution (an equilibrium of **8Zn** and **9Zn**) showed a sharp signal at g = 2.0022 with side bands. Variable temperature (VT) ESR spectra revealed the intensity of the side bands increases along with temperature (Figure 3d), clearly indicating the existence of high-spin species. Moreover, decreasing of the relative intensity of the side bands was observed at lower concentration (Figure S2-4 in the SI). Thus, the sharp signal around g = 2 can be attributed to the monomeric doublet species **8Zn**, and the side bands are attributed to the fine structures of the thermally excited triplet state of **9Zn**. In fact, these side bands were nicely reproduced by simulation by assuming S = 1, |D| = 132 MHz (44.03 cm^{-1}), and |E| = 20 MHz (6.67 cm^{-1}) (Figure 3e). These signals were completely changed to a sharp signal at g =

2.0020 (Figure 3f) upon addition of pyridine, which has been assigned as **8Zn-py**. The spin−spin distance has been estimated to be 8.6 Å on the basis of the D value, which is between the C(15)−C(15)′ length (12.4 Å) and the Zn−Zn′ length (5.7 Å), again indicating that two spins are present in the two porphyrin π-systems of **9Zn**.

The magnetic characters of **8H$_2$**, **8Ni**, **8Zn-py**, and **9Zn** in the solid (powder) states were also examined by their temperature dependent magnetic susceptibility with a superconducting quantum interference device (SQUID) apparatus (Figure 4). Curiously, the observed χT plots clearly indicated
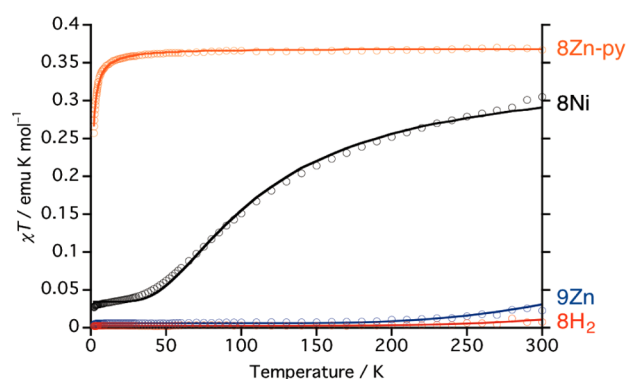

Figure 4. Observed $\chi T - T$ plots (circles) and simulated line of **8H$_2$** (red), **8Ni** (black), **8Zn-py** (orange), and **9Zn** (blue).

the different degrees of magnetic interaction. Although the magnetic analyses were conducted for powder samples, it may be considered that molecules should take packing structures similar to their single crystals in a microscopic sense. Namely, **8H$_2$**, **8Ni**, and **9Zn** take π-stacked dimeric structures while **8Zn-py** remains isolated from π-stacking in crystals. In addition, these π-radicals should interact magnetically through

the overlap of SOMO orbitals. Based on these assumptions, observed χT plots were properly reproduced with the Bleaney–Bowers singlet–triplet model[19] (eq 1) for dimeric radicals (**8H$_2$**, **8Ni**, and **9Zn**), and the Curie–Weiss model (eq 2) for isolated radical (**8Zn-py**). Fitted parameters are summarized in Table 1. Reflecting the high degree of π-stacking, **8H$_2$** displayed

Table 1. Parameters Simulated for 8H$_2$, 8Ni, 8Zn-py, and 9Zn

Compound	f_1	f_2	J_1/k_B	C	θ_p
8H$_2$	0.93	0.035	−790 K	–	–
8Ni	0.84	0.046	−101 K	–	–
8Zn-py	–	–	–	0.369	−0.77 K
9Zn	0.90	0.005	−720 K	–	–

strong exchange interaction with $J_1/k_B = -790$ K, while partially π-stacked **8Ni** showed moderate antiferromagnetic interaction with $J_1/k_B = -101$ K. **8Zn-py** behaved as a typical monoradical species with Curie constant $C = 0.369$ along with Weiss temperature $\theta_p = -0.77$ K. A χT plot of non-Kekulé molecule **9Zn** was also reproduced with the S-T model with $J_1/k_B = -720$ K, again confirming its singlet ground state.

$$\chi T = \frac{CT}{T - \theta_p}$$ (eq 1)

$$\chi T = f_1 \frac{N_A g^2 \mu_B^2}{k_B} \frac{1}{3 + \exp\left(-\frac{2J_1}{k_B T}\right)} + f_2 \frac{N_A g^2 \mu_B^2}{2k_B}$$ (eq 2)

Electrochemical Properties. The electrochemical properties of **8H$_2$**, **8Ni**, **8Zn-py**, and **9Zn** were studied by cyclic voltammetry in CH$_2$Cl$_2$ containing 0.1 M nBu$_4$NPF$_6$ as a supporting electrolyte (Figure 5). For **8Zn-py**, ca. 2% of pyridine was added to ensure the coordination of pyridine. The observed redox waves were fairly reversible, and their potentials are summarized in Table 2. All these radical species showed
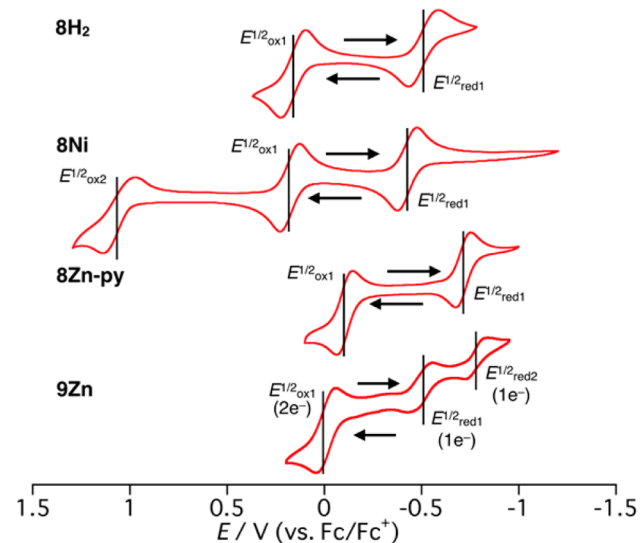

Figure 5. Cyclic voltammograms of **8H$_2$**, **8Ni**, **8Zn-py**, and **9Zn** in CH$_2$Cl$_2$ containing 0.1 M nBu$_4$NPF$_6$ as a supporting electrolyte versus the ferrocene/ferrocenium cation. Scan rate: 0.05 V s^{-1}; working electrode: Pt; counter electrode: Pt wire; reference electrode: Ag/0.01 M AgClO$_4$ in MeCN.

Table 2. Oxidation and Reduction Potentials of 8, 8Ni, 8Zn-py, and 9Zn in CH$_2$Cl$_2$ (vs Fc/Fc$^+$)

Compound	$E^{1/2}_{ox1}$/V	$E^{1/2}_{ox2}$/V	$E^{1/2}_{red1}$/V	$E^{1/2}_{red2}$/V	ΔE^b/V
8H$_2$	0.163	–	−0.534	–	0.697
8Ni	0.183	1.16	−0.446	–	0.629
8Zn-py^a	−0.105	–	−0.713	–	0.818
9Zn	0.052	–	−0.518	−0.819	0.570

^{a}In CH$_2$Cl$_2$ containing ca. 2% of pyridine. $^b\Delta E = E^{1/2}_{ox1} - E^{1/2}_{red1}$.

narrow gaps of around 0.7 V between the first oxidation and reduction waves, in line with their radical character. The oxidation and reduction potentials of **8Zn-py** are significantly lower than those in **8H$_2$** and **8Ni** due to the electron rich natures of the Zn(II) porphyrin coordinated with pyridine. The second oxidation wave was observed only for **8Ni**, which can be ascribed to the oxidation of the Ni(II) center. For dimer **9Zn**, a single two-electron oxidation wave at 0.052 V and two one-electron reduction waves at −0.518 ($E^{1/2}_{red1}$) and −0.819 V ($E^{1/2}_{red2}$) were observed. The difference ($E^{1/2}_{red1} - E^{1/2}_{red2}$) of the split reduction waves, 0.301 V, indicated relatively strong electronic interaction in the dimer and, hence, formation of a mixed-valent species.

Excited-State Dynamics. Femtosecond transient absorption (TA) measurements were carried out to investigate the excited state dynamics. The TA spectra of **7H$_2$**, **7Ni**, and **7Zn** showed typical spectral features of Ni(II) and Zn(II) porphyrins (Figure S9-1 in the SI).[20,21] The TA spectra of **8H$_2$**, **8Ni**, and **8Zn-py** decayed rapidly, with time constants of 0.6 and 9.8 ps for **8H$_2$**, 0.6 and 8.0 ps for **8Ni**, and 0.8 and 9.8 ps for **8Zn-py** (Figure S9-2 in the SI), which can be assigned as ultrafast internal conversion processes to the lowest excited state and deactivation processes to the open-shell ground state, respectively. These overall excited state dynamics governed by ultrafast relaxation dynamics indicate the high density of states, which is consistent with their radical character.[13,14] Compared to **8Zn-py**, **9Zn** showed a relatively large excited state absorption signal over 550 nm and accelerated decay processes with time constants of 0.36 and 6.5 ps. The faster relaxation dynamics of **9Zn** may be attributed to strong electronic interactions between the two stable porphyrin radicals.

Theoretical Calculations. Density functional theory (DFT) calculation[22] at the UB3LYP/6-311G(d)(C,H,N,O)-cc-pVQZ(Ni, Zn) level on these radicals revealed effective spin delocalization over the porphyrin macrocycle (Figure 6(a)). The diradical index y was also calculated for **9Zn** to be 0.86, indicating its large diradical character.[23] In contrast to the subporphyrin *meso*-oxy radical **5**, there is virtually no spin delocalization on the *meso*-aryl groups consistent with ESR studies. The calculated Mulliken atomic spin densities are summarized in Figures 6(b) and 6(c). In all cases, the largest spin densities of around 0.25 are found at the 15-positions of these radicals. This clearly indicates the most important resonance contributor is oxophlorin type one.

Time-dependent DFT (TD-DFT) calculations were also performed at the UB3LYP/6-311G(d)(C,H,N,O)-cc-pVQZ-(Ni,Zn) level. The lowest absorption bands were assigned to SOMO (singly occupied molecular orbital)−LUMO (lowest unoccupied molecular orbital) excitation (see SI) with small oscillator strengths $f = 0.0015$ (at 1021 nm) for **8H$_2$**, 0.0074 (at 1176 nm) for **8Ni**, and 0.0038 (at 1065 nm) for **8Zn-py**. Importantly, for the coordination dimer **9Zn**, the characteristic NIR absorption band is predicted at 1730 nm with large
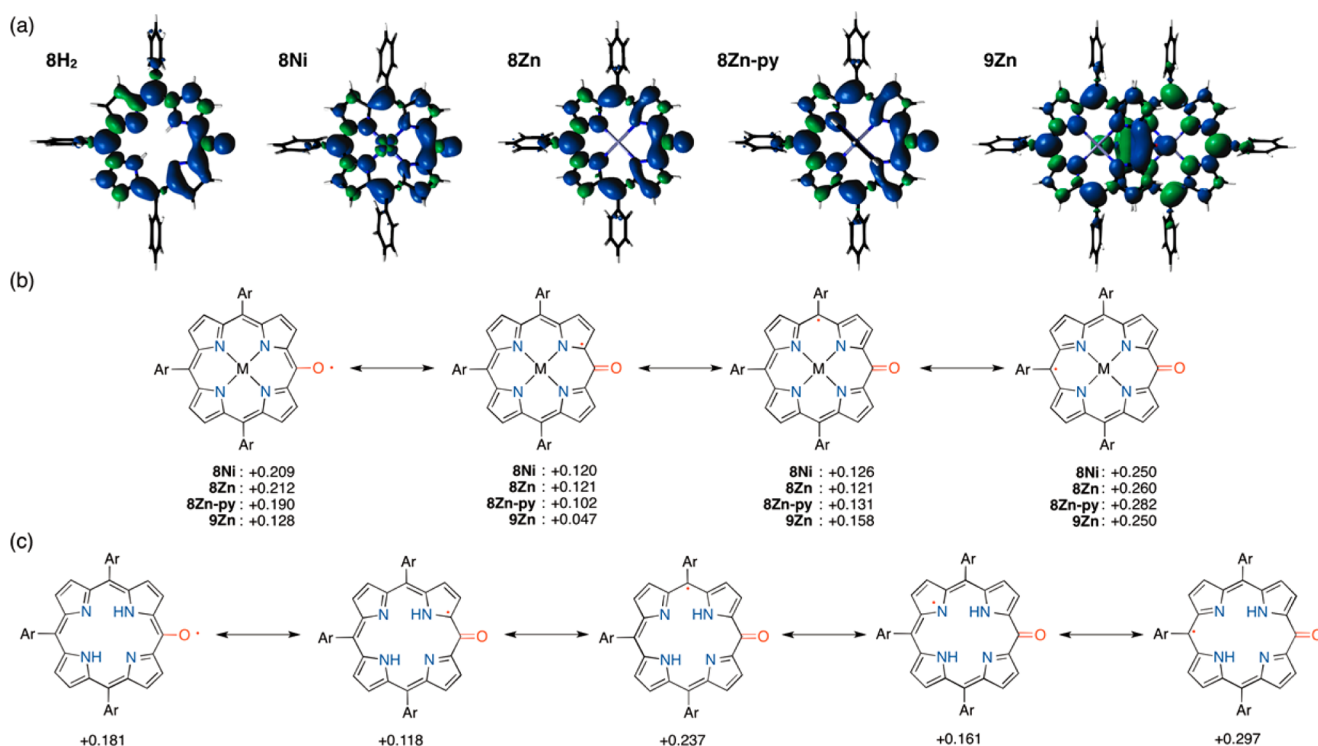
Figure 6. (a) Spin density distribution plots (isovalue: 0.01). (b) Atomic spin densities of **8Ni**, **8Zn-py**, and **9Zn** (bottom). (c) Atomic spin density of **8H₂**. Resonance contributors with spin density of less than 0.1 are not shown.

oscillator strength f = 0.2623 by TD-DFT calculation at the UCAM-B3LYP/6-311G(d)(C,H,N,O)-cc-pVQZ(Zn) level. The molecular orbital distribution involved in the lowest transition clearly indicates a charge transfer (CT) character in the coordination dimer **9Zn** (Figure 7). Usually CT absorption
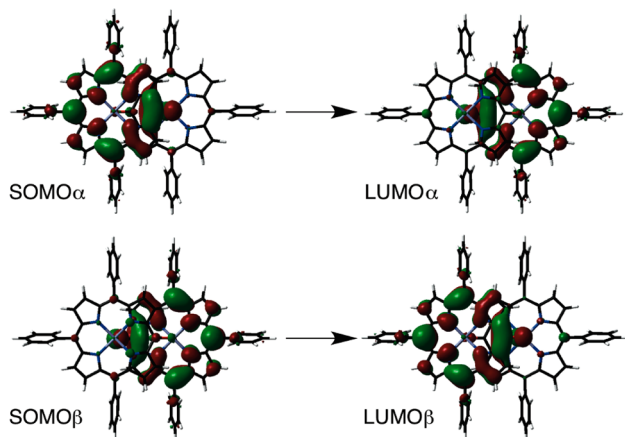

Figure 7. Molecular orbital profiles of the major electronic transition for the lowest energy transition of **9Zn** calculated at the UCAM-B3LYP/6-311G(d)-cc-pVQZ(Zn) level.

bands are unfavorable and very rare between the same chromophores,[24] since CT interaction needs the combination of an electron donor and an electron acceptor. However, such asymmetric CT bands have been observed for some π-radical species at high concentration both in solution and in the solid states.[25] This has been ascribed to their open-shell electronic natures, which allow for facile reduction and oxidation, as seen for the porphyrin *meso*-oxy radicals. In other words, such radicals can serve as a good donor and a good acceptor.

Moreover, in **9Zn**, the short interchromophore distance (3.112 Å) by the stable coordination dimeric radical system is considered to induce strong electronic interactions.

Synthesis of Oxophlorin π-Cations. The fairly reversible and low oxidation waves of these radical species encouraged us to isolate the corresponding oxophlorin cation species, which are, to the best of our knowledge, unprecedented in porphyrin chemistry. One-electron oxidation of **8Ni** and **8Zn** was accomplished upon treatment with tris(4-bromophenyl)-aminium hexachloroantimonate. Subsequent simple precipitation with CH₂Cl₂/n-hexane gave oxophlorin π-cations **10Ni** and **10Zn** as fairly stable salts with a hexachloroantimonate anion in 95% and 69% yield, respectively (Scheme 3).

Scheme 3. One-Electron Oxidation of 8Ni and 8Zn
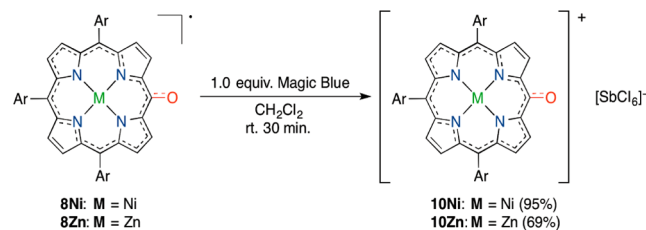
Unfortunately, their free-base derivative was not obtained from **8H₂** under similar reaction conditions, presumably due to easy deprotonation of the pyrrolic NH proton and subsequent degradation of the oxophlorin cation. The ¹H NMR spectra of both **10Ni** and **10Zn** show well-resolved peaks, confirming their closed-shell electronic structures. In addition, signals due to the pyrrolic β-protons are observed at higher fields: at 5.2–6.9 ppm for **10Ni** and at 5.7–6.9 ppm for **10Zn** as compared to those of *meso*-hydroxyporphyrins **7Ni** and **7Zn**, indicating a loss

of macrocyclic aromaticity of the porphyrin ring in **10Ni** and **10Zn**.

These oxophlorin cations are remarkably stable in non-nucleophilic solvents and in the solid-state. Single crystals of **10Ni** with counteranion $[SbCl_6]^-$ were obtained by slow vapor diffusion of *n*-hexane into a CH_2Cl_2 solution of **10Ni** under open air. X-ray diffraction analysis revealed its saddle-like structure with a C−O bond length of 1.209(7) Å, which is shorter than those of the radical species, indicating stronger double bond character (Figure 8a). The distance between the
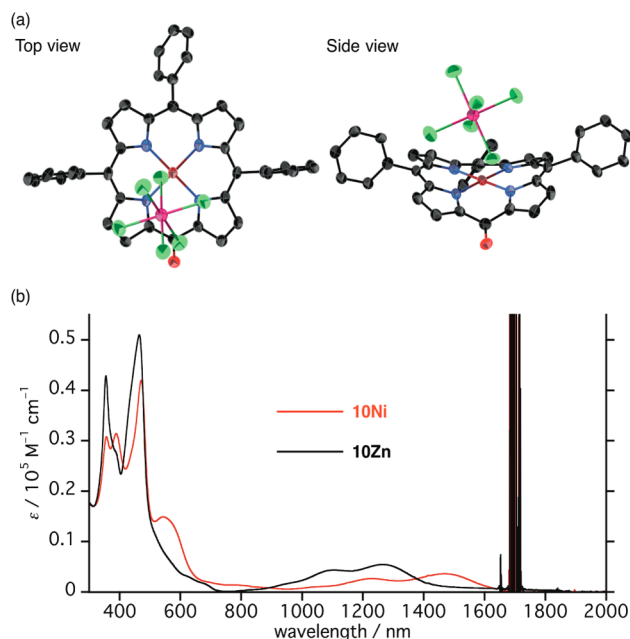

Figure 8. (a) X-ray crystal structure of **10Ni**. Thermal ellipsoids are scaled at the 50% probability level. Solvent molecules, hydrogen atoms, and *tert*-butyl groups are omitted for clarity. (b) UV/vis/NIR absorption spectra of **10Ni** (red) and **10Zn** (black) in CH_2Cl_2.

nearest chlorine atom of the counteranion and the central Ni atom is 3.117 Å, which is slightly shorter than the sum of van der Waals radii (3.38 Å), suggesting a certain coordination interaction.

The UV/vis absorption spectra of **10Ni** and **10Zn** are similar to those of the corresponding radical species (Figure 8b), but disappearance of the absorption band around 800 nm and growth of NIR absorption bands up to 1600 nm are characteristic for the oxophlorin cations. The lowest excited-state lifetimes of **10Ni** and **10Zn** were measured as 8 and 13 ps, respectively (Figure S9-3 in the SI), which is in good agreement with their nonradiative nature. DFT calculation on both **10Ni** and **10Zn** (calculated without counteranions) at the B3LYP/6-311G(d)(C,H,N,O)-cc-pVQZ(Ni,Zn) level revealed that a positive charge is delocalized over porphyrin macrocycle, and large positive atomic charges 0.30 (**10Ni**) and 0.32 (**10Zn**) were found at C(11) atoms. On the other hand, C(15) atoms, which have the largest spin density in **8Ni** and **8Zn**, have almost zero atomic charges in **10Ni** and **10Zn**. Moreover, the oxygen atoms have negative charges −0.24 (both **10Ni** and **10Zn**), indicating that there is no contribution of oxygen-centered cation character. TD-DFT calculation at the B3LYP/6-311G(d)(C,H,N,O)-cc-pVQZ(Ni,Zn) level was employed to assign their absorption spectra. The lowest excitation bands were assigned as the HOMO−LUMO transition with f =

0.0374 (at 1113 nm) for **10Ni** and 0.0543 (at 1029 nm) for **10Zn** (Figure S8-12,13 in the SI).

■ CONCLUSION

In summary, 10,15,20-triarylporphyrin *meso*-oxy radicals **8H₂**, **8Ni**, **8Zn-py**, and **9Zn** have been explored as extremely stable radicals by the oxidation of 5-hydroxy-10,15,20-triarylporphyrin with PbO_2. While the radicals **8H₂** and **8Ni** have been shown to exist as a monoradical in solution, Zn(II) porphyrin *meso*-oxy radical was isolated as a face-to-face dimer **9Zn** in the solid state but has been shown to be in equilibrium between monoradical **8Zn** and **9Zn** in noncoordinating solvents, depending upon concentration. Addition of pyridine to this solution led to the formation of pyridine-coordinated monoradical **8Zn-py**. SQUID measurements of these radicals revealed that their magnetic interactions are significantly influenced by the packing structures, and the antiferromagnetic interaction increases in the order of **8Zn-py** < **8Ni** < **9Zn** < **8H₂**, roughly reflecting the interporphyrin separations. These stable radicals underwent one-electron oxidation and reduction in a highly reversible manner within narrow windows of 0.57−0.82 V. Finally, **8Ni** and **8Zn** were oxidized with tris(4-bromophenyl)aminium hexachloroantimonate to produce corresponding oxophlorin π-cation species **10Ni** and **10Zn** for the first time, to the best of our knowledge. The structure of **10Ni** has been revealed to be saddle-like, similar to that of **8Ni**.

10,15,20-Triarylporphyrin *meso*-oxy radicals can be prepared easily in large scale, and their versatile fabrications will be possible. Considering the favorable attributes of porphyrins such as the intense absorption and emission in the visible and near-infrared regions, rich metal coordination chemistry, and facile formation of supramolecular aggregates, the stable radical species reported herein are quite promising building blocks in modular synthesis of covalently and noncovalently assembled oligomers possessing multiradical centers. We are also interested in exploration of other radicals stabilized by an electronic network of porphyrinoids, which are now actively pursued in our laboratory.

■ EXPERIMENTAL SECTION

Instrumentation and Materials. All reagents and solvents were of commercial reagent grade and were used without further purification unless where noted. Preparative separations were performed by silica gel column chromatography (Wako gel C-300). ¹H and ¹³C NMR spectra were recorded on a JEOL ECA-600 spectrometer, and chemical shifts were reported as the δ scale in ppm relative to the internal standards CHCl₃ (δ = 7.26 ppm for ¹H) or DMSO (δ = 2.50 ppm for ¹H and 39.52 ppm for ¹³C). CDCl₃ was purified by passing through a short aluminum oxide pad before use. ESR spectra for all samples were measured with a JEOL JES-FA200 spectrometer equipped with an OXFORD ESR900 He-flow cryostat. The measurement temperature was controlled with an OXFORD Mercury-iTC temperature controller. UV/vis/NIR absorption spectra were recorded on a Shimadzu UV-3600 spectrometer. Fluorescence spectra were recorded on a Shimadzu RD-5300PC spectrometer. Absolute fluorescence quantum yields were determined by the photon-counting method on a HAMAMATSU C9920-02S instrument. HR-APCI-TOF-MS and HR-ESI-TOF-MS spectra were recorded on a Bruker Daltonics micrOTOF LC instrument. X-ray crystallographic data were recorded on a Rigaku XtaLAB P-200 system by using graphite monochro-

matic Cu Kα radiation (λ = 1.54187 Å). The structures were solved by using direct methods (SIR-97[26] or SHELX-97[27]). Structure refinements were carried out by using SHELXL-98. CCDC numbers 1408586 (**7Ni**), 1408590 (**8H$_2$**), 1408587 (**8Ni**), 1408588 (**8Zn-py**), 1423041 (**9Zn**), and 1408589 (**10Ni**) contain supplementary crystallographic data for this paper. These data can be obtained free of charge from the Cambridge Crystallographic Data Centre via www.ccdc.cam.ac. uk/data_request/cif. Magnetic susceptibility was measured for powder samples in the temperature range from 2 to 300 K at 0.5 T magnetic fields with a Quantum Design MPMS-2S instrument. Redox potentials were measured by the cyclic voltammetry method on an ALS660 electrochemical analyzed model. Freshly distilled CH$_2$Cl$_2$ over CaH$_2$ was used for electrochemical analysis. Theoretical calculations were performed with the *Gaussian 09* package.[28]

meso-Hydroxyporphyrin Ni(II) Complex 7Ni. Following the reported procedure,[15] THF (120 mL) was added to a mixture of *meso*-bromoporphyrin **6Ni** (800 mg, 791 μmol), Cs$_2$CO$_3$ (1.9 g, 5.8 mmol, 7.4 equiv), Pd(OAc)$_2$ (12.4 mg, 55.2 μmol, 7 mol %), (R)-BINAP (52 mg, 84 μmol, 11 mol %), and (S)-BINAP (52 mg, 84 μmol, 11 mol %) in a 200 mL round-bottom flask under N$_2$. The reaction mixture was heated at 65 °C. After 48 h, the mixture was poured onto a saturated NH$_4$Cl solution and extracted with AcOEt. The organic layer was collected and dried over anhydrous Na$_2$SO$_4$. After removal of the solvent under reduced pressure, the crude mixture was purified by silica gel column chromatography (eluent: CH$_2$Cl$_2$:*n*-hexane = 1:1). A red fraction (R$_f$ ∼ 0.3) was collected. **7Ni** was recrystallized from CH$_2$Cl$_2$/MeOH (613 mg, 647 μmol, 82%). ^{1}H NMR (600 MHz, DMSO-d_6 with hydrazine monohydrate) δ/ppm = 8.39 (d, J = 4.6 Hz, 2H; β), 7.80 (d, J = 4.6 Hz, 2H; β), 7.67 (d, J = 4.6 Hz, 2H; β), 7.59 (t, J = 1.9 Hz, 2H; *meso*-Ar-*para*), 7.58 (d, J = 4.6 Hz, 2H; β), 7.55 (t, J = 1.9 Hz, 1H; *meso*-Ar-*para*), 7.54 (d, J = 1.9 Hz, 4H; *meso*-Ar-*ortho*), 7.52 (d, J = 1.9 Hz, 2H; *meso*-Ar-*ortho*), 1.39 (s, 36H; *t*Bu), 1.37 (s, 18H; *t*Bu); ^{13}C NMR (151 MHz, DMSO-d_6 with hydrazine monohydrate) δ/ppm = 165.2, 149.0, 148.8, 145.7, 143.2, 140.1, 140.0, 138.3, 137.3, 132.0, 127.8, 127.6, 127.0, 123.3, 120.5, 120.1, 109.6, 34.6, 31.5; UV−vis absorption (THF): λ_{max}/nm (ε/M^{-1} cm^{-1}) = 418 (2.6 × 10^5), 531 (1.5 × 10^4), and 572 (9.0 × 10^3); HRMS (APCI-TOF, positive mode): m/z calcd 947.5132 for [C$_{62}$H$_{73}$N$_4$O^{58}Ni]$^+$; [M + H]$^+$; found: 947.5085.

meso-Hydroxyporphyrin 7H$_2$. Sulfuric acid (5 mL) was added dropwise to an ice-cooled suspension of **7Ni** (100 mg, 105 μmol) in TFA (25 mL), and the resulting mixture was stirred at 0 °C. After 30 min, the reaction mixture was poured onto ice and neutralized with a sufficient amount of aqueous NaOH solution and NaHCO$_3$ solution. Product was extracted with CH$_2$Cl$_2$. Organic layers were collected and dried over anhydrous Na$_2$SO$_4$. The crude mixture was purified by silica gel column chromatography (eluent: first CH$_2$Cl$_2$, then AcOEt). A green fraction was obtained. **7H$_2$** was precipitated from MeOH as purple solids (90.5 mg, 102 μmol, 97%). ^{1}H NMR (600 MHz, DMSO-d_6 with hydrazine monohydrate) δ/ppm = 8.37 (d, J = 4.6 Hz, 2H; β), 7.68 (d, J = 4.6 Hz, 2H; β), 7.66 (broad s, 4H; *meso*-Ar-*ortho*), 7.62 (broad s, 2H; *meso*-Ar-*ortho*), 7.59 (broad s, 2H; *meso*-Ar-*para*), 7.56 (broad s, 1H; *meso*-Ar-*para*), 7.51 (d, J = 4.6 Hz, 2H; β), 7.40 (d, J = 4.6 Hz, 2H; β), 1.42 (s, 36H; *t*Bu), 1.39 (s, 18H; *t*Bu); ^{13}C NMR (151 MHz, DMSO-d_6 with hydrazine monohydrate) δ/ppm = 168.5, 158.6, 158.4, 149.1, 148.7, 141.4, 141.3, 128.1, 127.7, 121.8, 121.3, 120.4,

119.9, 118.4, 116.4, 114.4, 108.4, 34.7, 31.6; UV−vis absorption (THF): λ_{max}/nm (ε/M^{-1} cm^{-1}) = 418 (2.3 × 10^5), 489 (3.2 × 10^3), 522 (6.6 × 10^3), 559 (1.1 × 10^4), 662 (1.0 × 10^4); Fluorescence (THF, λ_{ex} = 420 nm): λ_{max} = 663, 727 nm (Φ_f = 0.064); HRMS (APCI-TOF, positive mode): m/z calcd 891.5935 for [C$_{62}$H$_{75}$N$_4$O]$^+$; [M + H]$^+$; found: 891.5913.

meso-Hydroxyporphyrin Zn(II) Complex 7Zn. *Method A: From meso-Bromo-Zn^{II}-porphyrin.* THF (30 mL) was added to a mixture of **6Zn** (350 mg, 344 μmol), Cs$_2$CO$_3$ (830 mg, 2.5 mmol, 7.4 equiv), Pd(OAc)$_2$ (5.4 mg, 24 μmol, 7 mol %), (R)-BINAP (23.9 mg, 36 μmol, 11 mol %), and (S)-BINAP (23.9 mg, 36 μmol, 11 mol %) under N$_2$ atmosphere. The mixture was heated at 65 °C. After 7 days, the reaction was quenched with saturated NH$_4$Cl solution and extracted with AcOEt. The organic layer was collected and dried over anhydrous Na$_2$SO$_4$. After removal of the solvent under reduced pressure, the crude mixture was purified by silica gel column chromatography (eluent: CH$_2$Cl$_2$:*n*-hexane = 1:4). A red fraction (**7Zn**; R$_f$ ∼ 0.3) and a brown fraction (**8Zn** or **9Zn**; R$_f$ ∼ 0.1) were collected. Both **7Zn** and **9Zn** were precipitated from hexane as purple and brown solids, respectively (**7Zn**: 66.2 mg, 69.3 μmol, 20%; **9Zn**: 22.4 mg, 23.5 μmol, 6.8%). ^{1}H NMR (600 MHz, DMSO-d_6 with hydrazine monohydrate) δ/ppm = 8.52 (d, J = 4.1 Hz, 2H; β), 7.74 (d, J = 4.6 Hz, 2H; β), 7.65 (d, J = 1.8 Hz, 4H; *meso*-Ar-*ortho*), 7.58 (d, J = 4.6 Hz, 2H ; β), 7.58 (d, J = 1.4 Hz, 2H, *meso*-Ar-*ortho*), 7.55 (t, J = 1.8 Hz, 2H; *meso*-Ar-*para*), 7.49 (m, 3H; *meso*-Ar-*para* + β), 1.37 (s, 36H; *t*Bu), 1.34 (s, 18H; *t*Bu); ^{13}C NMR (151 MHz, DMSO-d_6 with hydrazine monohydrate) δ/ppm =169.3, 154.5, 149.0, 148.8, 148.5, 146.5, 143.9, 143.1, 142.9, 131.7, 128.6, 128.2, 127.8, 123.6, 122.2, 122.0, 120.0, 119.4, 109.5, 34.9, 31.8; UV−vis absorption (THF): λ_{max}/nm (ε/M^{-1}cm^{-1}) = 424 (4.5 × 10^5), 561 (8.3 × 10^3), 618 (1.9 × 10^4); Fluorescence (THF, λ_{ex} = 424 nm): λ_{max} = 610, 678 nm (Φ_f = 0.081); HRMS (APCI-TOF, positive mode): m/z = calcd 952.4992 for [C$_{62}$H$_{72}$N$_4$O^{64}Zn]$^+$; [M]$^+$; found 952.4956.

Method B: From meso-Hydroxyporphyrin. A solution of Zn(OAc)$_2$ (12.3 mg, 56 μmol, 5 equiv) in MeOH (1 mL) was added to a solution of **7** (10.0 mg, 11.2 μmol) in CH$_2$Cl$_2$ (3 mL). The resulting mixture was stirred at room temperature for 2 h and then concentrated. The mixture was purified by silica gel column chromatography (eluent: CH$_2$Cl$_2$: *n*-hexane =1:4). A red fraction emitting red fluorescence when excited by handy UV-lamp was collected and **7Zn** was recrystallized from CH$_2$Cl$_2$/MeOH (8.8 mg, 9.3 μmol, 83%).

General Procedure for Oxidation of meso-Hydroxyporphyrins to the Corresponding Radicals. To a solution of *meso*-hydroxyporphyrin (1.0 equiv) in CH$_2$Cl$_2$, an excess amount of PbO$_2$ (ca. 800 equiv) was added and the resulting solution was stirred for 5 min at room temperature. After the reaction mixture was filtered through a short Celite pad, the solvent was removed under reduced pressure. The corresponding *meso*-oxy radical species were obtained by recrystallization from CH$_2$Cl$_2$/*n*-hexane.

meso-Oxy Radical 8H$_2$. According to the general procedure, **8H$_2$** (69.0 mg, 77.5 μmol, 86%) was obtained from **7H$_2$** (80.0 mg, 89.8 μmol) as brown solids. UV−vis absorption (CH$_2$Cl$_2$): λ_{max}/nm (ε/M^{-1}cm^{-1}) = 367 (5.1 × 10^4), 420 (9.7 × 10^4), 480 (1.8 × 10^4), 535 (1.0 × 10^4), 576 (1.1 × 10^4), 815 (1.7 × 10^4), 1123 (310), 1312 (950); HRMS (APCI-TOF, positive mode): m/z calcd 890.5857 for [C$_{62}$H$_{74}$N$_4$O]$^+$; [M + H]$^+$; found: 890.5827.

15592

J. Am. Chem. Soc. 2015, 137, 15584−15594

***meso*-Oxy Radical Ni(II) Complex 8Ni.** According to the general procedure, **8Ni** (91.1 mg, 96.2 μmol, 91%) was obtained from **7Ni** (100 mg, 106 μmol) as brown solids. UV−vis absorption (CH$_2$Cl$_2$): λ_{max}/nm (ε/M^{-1}cm^{-1}) = 351 (2.5 × 10^4), 437 (8.3 × 10^4), 497 (2.1 × 10^4), 582 (4.5 × 10^3), 807 (1.1 × 10^4) 1134 (160), 1332 (490), 1621 (110); HRMS (APCI-TOF, positive mode): m/z calcd 946.5054 for [C$_{62}$H$_{72}$N$_4$ONi]$^+$; [M + H]$^+$; found: 946.5074.

***meso*-Oxy Radical Zn(II) Complex Dimer 9Zn.** According to the general procedure, **9Zn** (17.6 mg, 18.5 μmol, 89%) was obtained from **7Zn** (20.0 mg, 20.9 μmol) as brown solids. UV−vis absorption [CH$_2$Cl$_2$, 1.68 × 10^{-5} M (total concentration based on monomer)]: λ_{max}/nm (ε/M^{-1}cm^{-1}) = 368 (3.3 × 10^4), 436 (8.2 × 10^4), 730 (4.9 × 10^3), 845 (5.7 × 10^3), 1415 (7.1 × 10^3); HRMS (ESI-TOF, negative mode): m/z = calcd 1902.9844 for [M]$^-$; [C$_{124}$H$_{142}$N$_8$O$_2$^{64}Zn$_2$]$^-$; found: 1902.9781.

***meso*-Oxy Radical Zn(II) Complex Pyridine Adduct 8Zn-py.** **8Zn-py** was recrystallized from a solution of **9Zn** (10.0 mg, 5.24 μmol) in CH$_2$Cl$_2$/pyridine/MeCN (10.7 mg, 10.4 μmol, quant.). UV−vis absorption (CH$_2$Cl$_2$ + 2% pyridine): λ_{max}/nm (ε/M^{-1}cm^{-1}) = 370 (4.0 × 10^4), 438 (1.2 × 10^5), 492 (2.0 × 10^4), 598 (7.5 × 10^3), 860 (1.7 × 10^4), 1149 (4.3 × 10^2), 1367 (1.4 × 10^3).

General Procedure for Oxidation of *meso*-Oxy Radicals to the Corresponding *meso*-Oxy Cations. To a solution of *meso*-oxy radical (1.0 equiv) in CH$_2$Cl$_2$ under N$_2$ atmosphere, tris(4-bromophenyl)aminium hexachloroantimonate (1.0 equiv) was added. The resulting mixture was stirred at room temperature for 30 min. Solvents were removed under reduced pressure. The corresponding oxophlorin cation species were obtained by recrystallization from CH$_2$Cl$_2$/n-hexane.

Oxophlorin Cation Ni(II) Complex Hexachloroantimonate 10Ni. According to the general procedure, **10Ni** (25.6 mg, 20.0 μmol, 95%) was obtained from **8Ni** (20.0 mg, 21.1 μmol) as brown solids. ^{1}H NMR (600 MHz, CDCl$_3$) δ/ppm =7.44 (broad s, 2H; *meso*-Ar-*ortho*), 7.40 (broad s, 1H; *meso*-Ar-*para*), 6.97 (broad s, 4H; *meso*-Ar-*ortho*), 6.88 (broad s, 2H; *meso*-Ar-*para*), 6.10 (d, J = 3.7 Hz, 2H; β), 5.87 (d, J = 3.7 Hz, 2H; β), 5.41 (d, J = 3.7 Hz, 2H; β), 5.29 (d, J = 3.7 Hz, 2H; β), 1.28 (s, 36H; *t*Bu), 1.26 (s, 18H; *t*Bu); (clear ^{13}C NMR spectrum was not obtained due to the broadness of signals); UV−vis absorption (CH$_2$Cl$_2$): λ_{max}/nm (ε/M^{-1}cm^{-1}) = 357 (3.1 × 10^4), 389 (3.1 × 10^4), 471 (4.2 × 10^4), 543 (1.5 × 10^4), 1227 (2.7 × 10^3), 1468 (3.6 × 10^3); HRMS (APCI-TOF, positive mode): m/z = calcd 946.5054 for [M + H]$^+$; [C$_{62}$H$_{72}$N$_4$ONi]$^+$; found: 946.5013.

Oxophlorin Cation Zn(II) Complex Hexachloroantimonate 10Zn. According to the general procedure, **10Zn** (9.3 mg, 7.2 μmol, 69%) was obtained from **9Zn** (10.0 mg, 5.2 μmol) as brown solids. ^{1}H NMR (600 MHz, CDCl$_3$) δ/ppm =7.48 (broad s, 2H; *meso*-Ar-*ortho*), 7.44 (broad s, 1H; *meso*-Ar-*para*), 7.07 (broad s, 4H; *meso*-Ar-*ortho*), 7.05 (broad s, 2H; *meso*-Ar-*para*), 6.81 (broad s, 2H; β), 6.33 (broad s, 2H; β), 5.91 (broad s, 2H; β), 5.79 (broad s, 2H; β), 1.32 (s, 36H; *t*Bu), 1.29 (s, 18H; *t*Bu); (clear ^{13}C NMR spectrum was not obtained due to the broadness of signals); UV−vis absorption (CH$_2$Cl$_2$): λ_{max}/nm (ε/M^{-1}cm^{-1}) = 355 (4.3 × 10^4), 465 (5.1 × 10^4), 1106 (4.4 × 10^3), 1264 (5.5 × 10^3) ; HRMS (APCI-TOF, positive mode): m/z = calcd 951.4914 for [M]$^+$; [C$_{62}$H$_{72}$N$_4$O^{64}Zn]$^+$; found: 951.4894.

Crystal Data for 7Ni. C$_{62}$H$_{72}$N$_4$NiO·CH$_3$OH, triclinic, space group $P-1$, a = 9.011(6) Å, b = 15.824(8) Å, c = 20.375(8) Å, α = 70.31(4)°, β = 86.42(5)°, γ = 87.73(5)°, V = 2730(2) Å^3, ρ_{calced} = 1.192 g·cm^{-3}, Z = 2, R_1 = 0.0984 [I > 2.0σ(l)], R_w = 0.3013 (all data), GOF = 1.040. CCDC 1408586.

Crystal Data for 8H$_2$. C$_{62}$H$_{73}$N$_4$O·CH$_2$Cl$_2$, triclinic, space group $P-1$, a = 11.665(2) Å, b = 15.633(3) Å, c = 15.927(4) Å, α = 104.962(7)°, β = 91.926(9)°, γ = 95.774(5)°, V = 2786.4(10) Å^3, ρ_{calced} = 1.162 g·cm^{-3}, Z = 2, R_1 = 0.0906 [I > 2.0σ(l)], R_w = 0.2763 (all data), GOF = 1.010. CCDC 1408590.

Crystal Data for 8Ni. C$_{62}$H$_{71}$N$_4$NiO, triclinic, space group $P-1$, a = 11.8998(18) Å, b = 16.0028(5) Å, c = 16.0810(6) Å, α = 64.42(3)°, β = 80.99(3)°, γ = 70.34(2)°, V = 2600.9(8) Å^3, ρ_{calced} = 1.209 g·cm^{-3}, Z = 2, R_1 = 0.0409 [I > 2.0σ(l)], R_w = 0.1171 (all data), GOF = 1.013. CCDC 1408587.

Crystal Data for 8Zn-py. C$_{67}$H$_{76}$N$_5$OZn·C$_6$H$_{14}$·C$_4$H$_8$O, triclinic, space group $P-1$, a = 13.2483(7) Å, b = 14.6134(10) Å, c = 18.0800(18) Å, α = 93.09(3)°, β = 104.28(4)°, γ = 116.22(2)°, V = 1989.4(4) Å^3, ρ_{calced} = 1.184 g·cm^{-3}, Z = 2, R_1 = 0.0842 [I > 2.0σ(l)], R_w = 0.2458 (all data), GOF = 1.032. CCDC 1408588.

Crystal Data for 9Zn. C$_{62}$H$_{71}$N$_4$OZn·C$_4$H$_8$O, triclinic, space group $P-1$, a = 12.5135(16) Å, b = 13.6400(11) Å, c = 18.3923(15) Å, α = 110.787(9)°, β = 99.471(14)°, γ = 95.73(2)°, V = 2852.0(6) Å^3, ρ_{calced} = 1.194 g·cm^{-3}, Z = 2, R_1 = 0.0453 [I > 2.0σ(l)], R_w = 0.1210 (all data), GOF = 1.026. CCDC 1423041.

Crystal Data for 10Ni. C$_{62}$H$_{71}$N$_4$NiO·Cl$_6$Sb·0.2(CH$_2$Cl$_2$), triclinic, space group $P-1$, a = 10.130(2) Å, b = 16.127(6) Å, c = 20.150(8) Å, α = 92.98(4)°, β = 97.03(6)°, γ = 105.76(8)°, V = 6883(3) Å^3, ρ_{calced} = 1.377 g·cm^{-3}, Z = 2, R_1 = 0.0570 [I > 2.0σ(l)], R_w = 0.1506 (all data), GOF = 1.003. CCDC 1408589.

ASSOCIATED CONTENT

Ⓢ Supporting Information

The Supporting Information is available free of charge on the ACS Publications website at DOI: 10.1021/jacs.5b11223.

Spectroscopic data, theoretical calculations, and cyclic voltammograms (PDF)
Cif data for **7Ni** (CIF)
Cif data for **8Ni** (CIF)
Cif data for **8H$_2$** (CIF)
Cif data for **8Zn-py** (CIF)
Cif data for **9Zn** (CIF)
Cif data for **10Ni** (CIF)

AUTHOR INFORMATION

Corresponding Authors
*kou-f@chem.sc.niigata-u.ac.jp
*dongho@yonsei.ac.kr
*osuka@kuchem.kyoto-u.ac.jp

Notes

The authors declare no competing financial interest.

ACKNOWLEDGMENTS

■ REFERENCES

(1) (a) Hicks, R. G., Ed. *Stable Radicals: Fundamentals and Applied Aspects of Odd-Electron Compounds*; Wiley-Blackwell: New York, 2010. (b) Hicks, R. G. *Org. Biomol. Chem.* **2006**, *5*, 1321.

(2) (a) Vogler, T.; Studer, A. *Synthesis* **2008**, *2008*, 1979. (b) Braunecker, W. A.; Matyjaszewski, K. *Prog. Polym. Sci.* **2007**, *32*, 93. (c) Lahti, P. M., Ed. *Magnetic Properties of Organic Materials*; Marcel Dekker: New York, 1999. (d) Morita, Y.; Nishida, S.; Murata, T.; Moriguchi, M.; Ueda, A.; Satoh, M.; Arifuku, K.; Sato, K.; Takui, T. *Nat. Mater.* **2011**, *10*, 947. (e) Raman, K. V.; Kamerbeek, A. M.; Mukherjee, A.; Atodiresei, N.; Sen, T. K.; Lazic, O.; Caciuc, V.; Michel, R.; Stalke, D.; Mandal, S. K.; Blügel, S.; Münzenberg, M.; Moodera, J. S. *Nature* **2013**, *493*, 509. (f) Rajca, A.; Wang, Y.; Boska, M.; Peletta, J. T.; Olankitwanit, A.; Swanson, M. A.; Mitchell, D. G.; Eaton, S. S.; Eaton, G. R.; Rajca, S. *J. Am. Chem. Soc.* **2012**, *134*, 15724.

(3) Clezy, P. S. In *The Porphyrins*, Vol. 2; Dolphin, D., Ed.; Academic Press: New York, 1978; p 103.

(4) (a) Yoshida, T.; Noguchi, M.; Kikuchi, G.; Sano, S. *J. Biochem.* **1981**, *90*, 125. (b) Sano, S.; Sano, T.; Morishima, I.; Shiro, Y.; Maeda, Y. *Proc. Natl. Acad. Sci. U. S. A.* **1986**, *83*, 531. (c) Wilks, A.; Ortiz de Montellano, P. R. *J. Biol. Chem.* **1993**, *268*, 22357. (d) Gossauer, A. *Chimia* **1994**, *48*, 352. (e) Matera, K. M.; Takahashi, S.; Fujii, H.; Zhou, H.; Ishikawa, K.; Yoshimura, T.; Rousseau, D. L.; Yoshida, T.; Ikeda-Saito, M. *J. Biol, Chem.* **1996**, *271*, 6618.

(5) (a) Warburg, O.; Negelein, E. *Ber. Dtsch. Chem. Ges. B* **1930**, *63*, 1816. (b) Balch, A. L.; Latos-Grażyński, L.; Noll, B. C.; Olmstead, M. M.; Szterenberg, L.; Safari, N. *J. Am. Chem. Soc.* **1993**, *115*, 1422. (c) Balch, A. L.; Latos-Grażyński, L.; Noll, B. C.; Olmstead, M. M.; Safari, N. *J. Am. Chem. Soc.* **1993**, *115*, 9056. (d) Balch, A. L.; Koerner, A. L.; Latos-Grażyński, L.; Lewis, L.; Claire, J. E. St.; Zovinka, T. N. *Inorg. Chem.* **1997**, *36*, 3892.

(6) Bonnett, R.; Dimsdale, M. J.; Sales, K. D. *J. Chem. Soc. D* **1970**, 962.

(7) (a) Balch, A. L.; Noll, B. C.; Zovinka, E. P. *J. Am. Chem. Soc.* **1992**, *114*, 3380. (b) Balch, A. L.; Noll, B. C.; Phillips, S. L.; Reid, S. M.; Zovinka, E. P. *Inorg. Chem.* **1993**, *32*, 4730. (c) Balch, A. L.; Mazzanti, M.; Olmstead, M. M. *Inorg. Chem.* **1993**, *32*, 4737.

(8) Balch, A. L. *Coord. Chem. Rev.* **2000**, *200−202*, 349.

(9) Fuhrhop, J.-H.; Besecke, S.; Subramanian, J.; Mengersen, C.; Riesner, D. *J. Am. Chem. Soc.* **1975**, *97*, 7141.

(10) Khoury, R. G.; Jaquinod, L.; Shachter, A. M.; Nelson, N. Y.; Smith, K. M. *Chem. Commun.* **1997**, 215.

(11) Khoury, R. G.; Jaquinod, L.; Paolesse, R.; Smith, K. M. *Tetrahedron* **1999**, *55*, 6713.

(12) Szterenberg, L.; Latos-Grażyński, L.; Wojaczyński, J. *ChemPhysChem* **2002**, *3*, 575.

(13) Koide, T.; Kashiwazaki, G.; Suzuki, M.; Furukawa, K.; Yoon, M.-C.; Cho, S.; Kim, D.; Osuka, A. *Angew. Chem., Int. Ed.* **2008**, *47*, 9661.

(14) Shimizu, D.; Oh, J.; Furukawa, K.; Kim, D.; Osuka, A. *Angew. Chem., Int. Ed.* **2015**, *54*, 6613.

(15) Esdaile, L. J.; Senge, M. O.; Arnold, D. P. *Chem. Commun.* **2006**, 4192.

(16) Similar phenomena were reported for *meso*-hydroxy porphyrin[15] and subporphyrin.[14]

(17) The similar coordination chemistry of 5-hydroxy-10,15,20-triarylporphyrin with various M(III) has been reported. (a) Wojaczyński, J.; Latos-Grażyński, L. *Inorg. Chem.* **1995**, *34*, 1044. (b) Wojaczyński, J.; Latos-Grażyński, L. *Inorg. Chem.* **1995**, *34*, 1054. (c) Wojaczyński, J.; Latos-Grażyński, L. *Inorg. Chem.* **1995**, *34*, 1044. (d) Wojaczyński, J.; Latos-Grażyński, L.; Olmstead, M. M.; Balch, A. L. *Inorg. Chem.* **1997**, *36*, 4548. (e) Balch, A. L.; Noll, B. C.; Olmstead, M. M.; Reid, S. M. *J. Chem. Soc., Chem. Commun.* **1993**, 1088. (f) Lee, H. M.; Olmstead, M. M.; Gross, G. G.; Balch, A. L. *Cryst. Growth Des.* **2003**, *3*, 691.

(18) Interplane distances were calculated as the distance between the mean planes, defined by 24 atoms of the porphyrin core.

(19) Bleaney, B.; Bowers, K. D. *Proc. R. Soc. London, Ser. A* **1952**, *214*, 451.

(20) (a) Retsek, J. L.; Drain, C. M.; Kirmaier, C.; Nurco, D. J.; Medforth, C. J.; Smith, K. M.; Sazanovich, I. V.; Chirvony, V. S.; Fajer, J.; Holten, D. *J. Am. Chem. Soc.* **2003**, *125*, 9787. (b) Yoon, M.-C.; Lee, S.; Tokuji, S.; Yorimitsu, H.; Osuka, A.; Kim, D. *Chem. Sci.* **2013**, *4*, 1756.

(21) Kim, K. S.; Lim, J. M.; Myśliborski, R.; Pawlicki, M.; Latos-Grażyński, L.; Kim, D. *J. Phys. Chem. Lett.* **2011**, *2*, 477.

(22) Theoretical calculations were performed based on X-ray crystal structures in which all *tert*-butyl groups were replaced by hydrogen atoms for simplicity. Since X-ray crystal structures of **8Zn** and **10Zn** were not obtained, their geometries were optimized from the X-ray structures of their Ni(II) derivatives.

(23) Diradical index y was calculated from the calculated occupation number n of UHF natural orbitals; $y = 1 - 2T/(1 + T^2)$, where $T = (n_{HOMO} - n_{LUMO})/2$.

(24) Selected papers for asymmetric charge transfer. (a) Wu, Y.; Young, R. M.; Frasconi, M.; Schneebeli, S. T.; Spenst, P.; Gardner, D. M.; Brown, K. E.; Würthner, F.; Stoddart, J. F.; Wasielewski, M. R. *J. Am. Chem. Soc.* **2015**, *137*, 13236. (b) Whited, M. T.; Patel, N. M.; Roberts, S. T.; Allen, K.; Djurovich, P. I.; Bradforth, S. E.; Thompson, M. E. *Chem. Commun.* **2012**, *48*, 284. (c) Trinh, C.; Kirlikobali, K.; Das, S.; Ener, M. E.; Gray, H. B.; Djurovich, P.; Bradforth, S. E.; Thompson, M. E. *J. Phys. Chem. C* **2014**, *118*, 21834.

(25) Selected papers for asymmetric charge transfer between radical species. In solutions: (a) Hausser, K. H.; Murrell, J. N. *J. Chem. Phys.* **1957**, *27*, 500. (b) Itoh, M.; Nagakura, S. *J. Am. Chem. Soc.* **1967**, *89*, 3959. (c) Maeda, K.; Hayashi, T. *Bull. Chem. Soc. Jpn.* **1969**, *42*, 3509. (d) Kimura, K.; Yamazaki, T.; Katsumata, S. *J. Phys. Chem.* **1971**, *75*, 1768. In solid states: (e) Goto, K.; Kubo, T.; Yamamoto, K.; Nakasuji, K.; Sato, K.; Shiomi, D.; Takui, T.; Kubota, M.; Kobayashi, T.; Yakusi, K.; Ouyang, J. *J. Am. Chem. Soc.* **1999**, *121*, 1619.

(26) Altomare, A.; Burla, M. C.; Camalli, M.; Cascarano, G. L.; Giaco-vazzo, C.; Guagliardi, A.; Moliterni, A. G. G.; Polidori, G.; Spagna, R. *J. Appl. Crystallogr.* **1999**, *32*, 115.

(27) (a) SHELXL-97, Program for the Refinement of Crystal Structures from Diffraction Data; University of Göttingen: Göttingen, Germany, 1997. (b) Sheldrick, G. M.; Schneider, T. R. *Methods Enzymol.* **1997**, *277*, 319.

(28) *Gaussian 09*, Revision A.02; Frisch, M. J.; Trucks, G. W.; Schlegel, H. B.; Scuseria, G. E.; Robb, M. A.; Cheeseman, J. R.; Scalmani, G.; Barone, V.; Mennucci, B.; Petersson, G. A.; Nakatsuji, H.; Caricato, M.; Li, X.; Hratchian, H. P.; Izmaylov, A. F.; Bloino, J.; Zheng, G.; Sonnenberg, J. L.; Hada, M.; Ehara, M.; Toyota, K.; Fukuda, R.; Hasegawa, J.; Ishida, M.; Nakajima, T.; Honda, Y.; Kitao, O.; Nakai, H.; Vreven, T.; Montgomery, J. A., Jr.; Peralta, J. E.; Ogliaro, F.; Bearpark, M.; Heyd, J. J.; Brothers, E.; Kudin, K. N.; Staroverov, V. N.; Kobayashi, R.; Normand, J.; Raghavachari, K.; Rendell, A.; Burant, J. C.; Iyengar, S. S.; Tomasi, J.; Cossi, M.; Rega, N.; Millam, J. M.; Klene, M.; Knox, J. E.; Cross, J. B.; Bakken, V.; Adamo, C.; Jaramillo, J.; Gomperts, R.; Stratmann, R. E.; Yazyev, O.; Austin, A. J.; Cammi, R.; Pomelli, C.; Ochterski, J. W.; Martin, R. L.; Morokuma, K.; Zakrzewski, V. G.; Voth, G. A.; Salvador, P.; Dannenberg, J. J.; Dapprich, S.; Daniels, A. D.; Farkas, Ö.; Foresman, J. B.; Ortiz, J. V.; Cioslowski, J.; Fox, D. J. Gaussian, Inc.: Wallingford, CT, 2009.